A Study of Binary Phospholipid Mixtures at the Air−Water Interface Using Infrared Reflection−Absorption Spectroscopy and 2D IR *βν* Correlation Analysis[†]

Douglas L. Elmore, Saratchandra Shanmukh, and Richard A. Dluhy*

University of Georgia, Department of Chemistry, Athens, Georgia 30602-2556

Received: July 2, 2001; In Final Form: October 25, 2001

Infrared reflection−absorption spectroscopy (IRRAS) in combination with isotopic substitution and a modified 2D IR correlation analysis procedure were used to study the dynamics of phospholipid acyl chain structure in both an ideal and a nonideal binary monolayer mixture spread at the air−water (A/W) interface. The ideal mixture consisted of a 1:2 molar ratio of 1,2-dipalmitoyl-*sn*-glycero-3-phosphocholine (DPPC) and 1,2-dipalmitoyl-d_{62}-*sn*-glycero-3-phosphocholine (DPPC-d_{62}), whereas the nonideal mixture consisted of a 1:2 molar ratio of 1,2-dilignoceroyl-*sn*-glycero-3-phosphocholine (DLiPC) and DPPC-d_{62}. The IRRAS spectra were interpreted using standard 2D IR methods as well as a modified two-dimensional correlation analysis called *βν* correlation analysis. In a *βν* correlation analysis, the effective phase angle (β_e) is determined for the signal variations in a discrete set of dynamic spectra at each spectral frequency. The β_e values are then used to quantitatively establish the relative rates of intensity change (i.e., the temporal relationships) as well as the degree of coherence between signal variations. In this study, similar β_e values are observed for the methyl and the methylene stretching bands in the DPPC component of the ideal mixture. This same behavior is observed for the methyl and the methylene stretching bands of the DPPC-d_{62} component in the ideal mixture and the DPPC-d_{62} component in the nonideal mixture. In contrast, dissimilar β_e values are observed for the methyl and the methylene stretching bands of the DLiPC component of the nonideal mixture. This observation can be explained by considering the location of gauche defects in the acyl chains of the individual components. As the mixed monolayer is compressed, conformational ordering takes place throughout the acyl chains of DPPC and DPPC-d_{62}, whereas ordering in the condensed phase DLiPC component is localized near the terminal methyl groups of the acyl chains. Methyl (2940 cm^{-1}) and methylene ($\sim$2890 cm^{-1}) Fermi resonance bands are clearly resolved from the fundamental bands in the C−H stretching region of the *βν* plot for the nonideal mixture. Average β_e values for the symmetric and antisymmetric methylene stretching vibrations were used to determine the relative rates of conformational ordering in the individual components of the two monolayer systems. The relative rates of ordering are summarized as DPPC in the ideal mixture ($\beta_e = 220°$) $\approx$ DPPC-d_{62} in the ideal mixture ($\beta_e = 218°$) > DPPC-d_{62} in the nonideal mixture ($\beta_e = 194°$) > DLiPC in the nonideal mixture ($\beta_e = 170°$). This study demonstrates for the first time that methyl stretching modes in IRRAS spectra can be used as in situ indicators of structural dynamics in the acyl chains of a Langmuir monolayer.

Introduction

Two-dimensional infrared spectroscopy (2D IR) is a mathematical technique for obtaining information that may not be obvious in conventional IR spectra.[1−4] There have recently been a variety of reports concerning the ability of 2D IR to provide enhanced spectral resolution, identify molecular details, and facilitate band assignments.[5−8] A smaller number of reports have appeared in which 2D IR has been used to establish the dynamic relationships among molecular groups in a molecule undergoing sample perturbation.[9−12] Although it is possible to establish the temporal relationships, or relative rates of change, among molecular groups in a dynamic data set using 2D IR, such an approach relies on a qualitative description of the sign of cross-peaks as determined by the phase angle between the two dynamic IR signals.[1] If the two dynamic IR signals vary according to an arbitrary waveform, as is often the case, the

exact phase angle can be determined only by methods that require a great deal of computational difficulty.[3,13]

We have recently introduced a modified two-dimensional infrared correlation method called *βν* correlation analysis.[14] The goal of a *βν* correlation analysis is to establish a simplified methodology for identifying relative rates of change or temporal relationships within a dynamic set of IR spectra. This procedure seeks to avoid the computational difficulties inherent in the exact calculation of the phase angles, yet it provides a more quantitative approach to describing the dynamic temporal relationships than by simply relying on the signs of 2D IR cross-peaks. In *βν* correlation analysis, an effective phase angle (β_e) is determined for the signal variations in a discrete set of dynamic spectra at each spectral frequency. The β_e values are then used to quantitatively establish the relative rates of intensity change and the degree of coherence between signal variations. (Although the term "relative rates" is used, no direct kinetic variables are measured. Technically, it is the relative sequence of events that is determined in a *βν* correlation analysis.)

A Study of Binary Phospholipid Mixtures

J. Phys. Chem. A, Vol. 106, No. 14, 2002 **3421**

In this article, we describe the first application of $\beta\nu$ correlation analysis to the IR spectra of monomolecular films at the air−water (A/W) interface. Infrared reflection−absorption spectroscopy (IRRAS) at the A/W interface has been widely used for in situ characterization of insoluble monolayer films spread at the A/W interface.[15−22] Furthermore, these so-called Langmuir monolayers often serve as excellent model systems of biological membranes.[23,24] These two facts help explain why IRRAS at the A/W interface has become such a popular technique for the study of membrane-mimetic monolayers.[25−28] The technique is quite powerful in the sense that it provides structural information about all parts of the amphipathic molecule. Furthermore, because IR absorption is sensitive to the displacement of the dipole transition moments, IRRAS can provide information about conformation and molecular tilt angles.[25,29] Unfortunately, the technique suffers from the fact that condensed-phase IRRAS vibrational bands are frequently broad and overlapping, complicating the assignment of structure to the observed vibrations. In addition, the structural dynamics, or relative rates of motion, of monolayer components have not been discernible using IRRAS techniques.

We have previously shown that standard 2D IR can be successfully applied to identifying the underlying band shapes in the broad, overlapping bands obtained in monolayer IRRAS spectra.[30,31] In this current report, we test whether $\beta\nu$ correlation analysis can be successfully applied to the study of structural dynamics in monolayer IRRAS spectra. To accomplish this, we have chosen to study two different binary phospholipid systems, representing both a thermodynamically ideal and nonideal mixture. The first binary mixture consists of a 1:2 molar ratio of 1,2-dipalmitoyl-*sn*-glycero-3-phosphocholine (DPPC; C16 acyl chains) and 1,2-dipalmitoyl-d_{62}-*sn*-glycero-3-phosphocholine (DPPC-d_{62}; C16 acyl chains); this mixture provides a thermodynamically ideal system. The second binary mixture consists of a 1:2 molar ratio of 1,2-dilignoceroyl-*sn*-glycero-3-phosphocholine (DLiPC; C24 acyl chains) and 1,2-dipalmitoyl-d_{62}-*sn*-glycero-3-phosphocholine (DPPC-d_{62}; C16 acyl chains); this mixture provides a thermodynamically nonideal system. The results from these studies show that, by applying 2D IR $\beta\nu$ correlation analysis, acyl chain structural dynamics can be followed by monitoring the methyl and methylene stretching bands in IRRAS spectra at the A/W interface.

Materials and Methods

Surface Chemistry. The synthetic phospholipids DPPC, DPPC-d_{62}, and DLiPC were obtained from Avanti Polar Lipids (Alabaster, AL) at 99+% stated purity and used without further purification. Subphase water was obtained from a Barnstead (Dubuque, IA) ROpure/Nanopure reverse osmosis/deionization system and had a nominal resistivity of 18.3 MΩ cm and a pH of approximately 5.6.

The 1:2 (mol:mol) DPPC/DPPC-d_{62} and 1:2 (mol:mol) DLiPC/DPPC-d_{62} solutions were prepared by dissolving the required amounts of each lipid in 9:1 (vol:vol) chloroform/methanol (Baker, HPLC grade) to produce 1.0 mg/mL solutions as DPPC-d_{62}. Lipid samples were spread onto a Nima 601M Series Langmuir film balance (Nima, Coventry, England) with an initial surface pressure of 0.5 mN/m and allowed to settle for 1 h before compression began.

Infrared Reflection−Absorption Measurements. The IRRAS spectra were collected using a Perkin-Elmer Spectrum 2000 FT-IR spectrometer (Perkin-Elmer, Norwalk, CT). The optical interface of the IR spectrometer to the Langmuir film

balance was designed in our laboratory. The IR beam coming from the spectrometer's external beam port reflected off a 60° gold-coated off-axis parabolic mirror (Janos Technology Inc., Townshend, VT), and through an infrared band-pass filter (OCLI, Santa Rosa, CA) onto the surface of the Nima film balance, resulting in an incidence angle of 30° to the surface normal. The IR beam reflected off of the subphase, sampling the film, and was recollimated by a second parabolic mirror that directed it onto the focusing mirror of a liquid-nitrogen--cooled narrow-band HgCdTe detector. The IR band-pass filter (3300−2000 cm^{-1}) was placed just above the water to reduce any localized heating effect.[32] The film balance, optical components, and detector are housed in a sealed Plexiglas chamber that allows humidity control of the local trough environment thus improving water vapor background subtraction.

A single beam spectrum of a pure water subphase was used as the background spectrum. The subphase temperature was held constant at 20 ± 1 °C by flowing thermostated water through the hollow body of the trough. The temperature in the enclosed chamber was approximately 22 °C with a relative humidity of approximately 65%. The monolayer film was compressed intermittently and spectra collected over a range of surface pressures from 1.0 mN/m to a maximum of 51.0 mN/m. The surface pressures ranging from 9.0 to 25.0 mN/m were used in the correlation analysis for both the ideal and nonideal monolayer mixtures.

IRRAS spectra were collected with 1024 scans each at 16 cm^{-1} resolution, apodized with a triangular function, and Fourier transformed with three levels of zero filling. The measurement time for 1024 scans was about 4.5 min. All monolayer IRRAS spectra are presented as reflection−absorbance spectra, i.e., $A = -\log(R/R_0)$, where R is the IR reflectivity of the monolayer-covered surface, and R_0 is the IR reflectivity of the bare water subphase background. A two-point baseline correction was applied to both the C−H and the C−D stretching regions of each spectrum using the GRAMS/32 program (Galactic Industries, Salem, NH). Adjustments for changes in surface density (i.e., intensity normalization) were also performed using GRAMS/32. As a reference point, the signal-to-noise ratio (SNR) of the CH$_2$ ν_a band (~2920 cm^{-1}) of the DPPC component of the ideally mixed monolayer was ~200:1 peak to peak at the highest surface pressures. Band positions were determined using the center-of-gravity algorithm described by Cameron et al.[33]

Calculation of 2D IR Correlation Spectra. The 2D IR synchronous spectrum, $\Phi(\nu_1,\nu_2)$, and the asynchronous spectrum, $\Psi(\nu_1,\nu_2)$, were calculated using eqs 1 and 2. These algorithms use the most recent mathematical formalism in which a Hilbert transform is utilized for calculating the asynchronous spectrum.[34] In all cases, the average spectrum was subtracted from each sequentially obtained surface pressure-dependent IRRAS spectrum to produce a set of dynamic IR spectra. The dynamic spectra were then used in the correlation analysis.

$$\Phi(\nu_1,\nu_2) = \frac{1}{N-1}\sum_{j=0}^{N-1} y(\nu_1,n_j)\, y(\nu_2,n_j) \tag{1}$$

$$\Psi(\nu_1,\nu_2) = \frac{1}{N-1}\sum_{j=0}^{N-1} y(\nu_1,n_j)\sum_{k=0}^{N-1} M_{jk}\, y(\nu_2,n_k) \tag{2}$$

In eqs 1 and 2, ν_1 and ν_2 represent two independent frequencies, n_j represents the number of the spectrum in the ordered sequence where the first spectrum number is zero, N represents the total number of spectra used in the calculation,

and M_{jk} is the Hilbert transform matrix, which is defined in eq 3:

$$M_{jk} = \begin{cases} 0 & \text{if } j = k \\ 1/\pi(k-j) & \text{otherwise} \end{cases} \qquad (3)$$

The 2D IR correlation analysis algorithms and 2D plots presented in this article were programmed in our laboratory using the MATLAB programming environment (version 6, The MathWorks, Inc., Natick, MA).

βν **Correlation Analysis.** A *βν* correlation analysis is a mathematical asynchronous cross correlation performed on a set of dynamically varying IR spectra against a set of sinusoidal functions that differ only by their phase angle β. A full description of the details of the *βν* correlation analysis have been presented elsewhere.[14] This type of correlation analysis is mathematically described using eq 4:

$$\Psi(\nu,\beta) = \frac{1}{N-1}\sum_{j=0}^{N-1} y(\nu,n_j) \sum_{k=0}^{N-1} M_{jk} \sin(k\phi + \beta) \qquad (4)$$

The correlation intensity Ψ at some point (ν,β) represents the correlation of the measured IR spectral intensity $y(\nu,n_j)$ with the mathematical function $\sin(k\phi + \beta)$. In eq 4, y is the IR intensity, ν is the frequency or wavenumber, n_j is the number of the spectrum in the ordered sequence where the first spectrum number is zero, β is the phase angle of the respective sine function, N is the total number of spectra used in the calculation, ϕ is a constant value in degrees (or radians) chosen based upon the total number of dynamic spectra used in the calculation, and M_{jk} is the Hilbert transform matrix previously defined in eq 3.

In this study all *βν* correlations were performed with $\phi = 10°$, so that $\sin(k10° + \beta)$ describes approximately $^1/_4$ of the cycle of a sine function or the approximate form of a commonly observed variation in spectral band intensities upon sample perturbation. Only the asynchronous correlation algorithm is used in the *βν* correlation analysis presented here, because asynchronous 2D IR correlations are more sensitive to differences in the form of the signal variation than are synchronous correlations.[1] Note also that the computational algorithm for the *βν* correlation analysis uses the most recent mathematical formalism, in which a Hilbert transform is used for calculating the asynchronous spectrum, rather than the more computationally cumbersome Fourier transform.[34]

The effective phase angle, β_e, is defined by eq 5:

$$\beta_e = \beta + 90° \qquad (5)$$

In eq 5, β is the point of maximum positive correlation intensity in the plot of β vs ν as defined by eq 4. The value of β_e is defined in this fashion so that the phase angle β and the effective phase angle β_e are the same for a sinusoidal signal variation with constant frequency. In this paper, the contour levels are evenly spaced in the *βν* plots from 0 to the maximum value for positive correlations. Negative correlations are not displayed because they simply differ from the positive correlations by 180°.

The *βν* algorithms for calculating effective phase angles as well as the plots of the resulting effective phase angles vs wavenumber were programmed in our laboratory using the MATLAB programming environment.

Results and Discussion

Figures 1 and 2 present the IRRAS spectra used for the 2D IR and *βν* calculations of the binary mixtures described in this
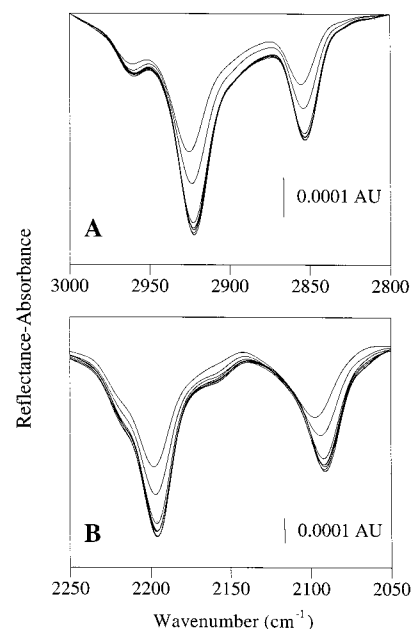

Figure 1. IRRAS spectra of the ideal binary monolayer (1:2 DPPC/DPPC-d$_{62}$) spread at the air−water interface. The spectra were collected as a function of monolayer surface pressure and have been normalized for changes in surface density. (A) The C−H stretching region representing the DPPC component in the binary monolayer. (B) The C−D stretching region representing the DPPC-d$_{62}$ component in the binary monolayer.
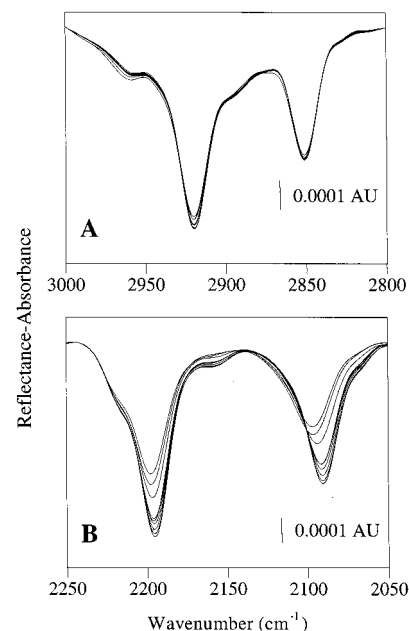

Figure 2. IRRAS spectra of the nonideal binary monolayer (1:2 DLiPC/DPPC-d$_{62}$) spread at the air−water interface. The spectra were collected as a function of monolayer surface pressure and have been normalized for changes in surface density. (A) The C−H stretching region representing the DLiPC component in the binary monolayer. (B) The C−D stretching region representing the DPPC-d$_{62}$ component in the binary monolayer.

article. All of the IRRAS spectra presented here were collected using an unpolarized incident IR beam and have been normalized for changes in surface density. The negative reflection−absorption bands seen in Figures 1 and 2 are observed in IRRAS spectra collected at the A/W interface for a 30° angle of incidence and are theoretically predicted by classical electromagnetic theory.[16,18,35] At an angle of incidence of 30°, the

A Study of Binary Phospholipid Mixtures

J. Phys. Chem. A, Vol. 106, No. 14, 2002 **3423**

reflectivity of s-polarized light at the A/W interface is about three times greater than that for p-polarized light. (For s-polarized light, the electric field is parallel to the plane of the aqueous serface. For p-polarized light, the electric field is parallel to the plane defined by the surface normal and the propagation direction of the light wave.) The IRRAS spectra are therefore ~75% s-polarized.[16,36] To acquire these spectra, the monolayer film was formed, allowed to equilibrate, and then compressed stepwise over a range of surface pressures from 9.0 to 25.0 mN/m with spectra collected during the interval between each successive compression. This surface pressure range includes the liquid expanded to liquid condensed (LE−LC) phase transition and a portion of the LC phase for both the ideal and nonideal monolayer mixtures.

The two binary phospholipid systems chosen for study represent a thermodynamically ideal and nonideal mixture, respectively. The first binary mixture consists of a 1:2 molar ratio of DPPC (C16 acyl chains) and DPPC-d_{62} (C16 acyl chains); this mixture provides a thermodynamically ideal system. The DPPC/DPPC-d_{62} system is miscible in all mole ratios because of the identical chain length of the two components.[37−39] The second binary mixture consists of a 1:2 molar ratio of DLiPC (C24 acyl chains) and DPPC-d_{62} (C16 acyl chains); this mixture provides a thermodynamically nonideal system. Gel state immiscibility in the DLiPC/DPPC-d_{62} system is predicted from the acyl chain length mismatch of the two components.[37−39]

IRRAS offers several advantages for the study of binary monolayer films. In particular, if one component of the mixture is isotopically labeled, the conformation of each component may be simultaneously monitored via IR spectroscopy. Such an approach has been applied to phospholipids, where the synthetic incorporation of perdeuterated acyl chains allows the monitoring of the conformationally sensitive C−D stretching bands in the same manner as that of the C−H region.[40,41] Substitution of deuterium for hydrogen results in a wavenumber shift of ~$2^{1/2}$ for the perdeuterated C−D bands, as predicted by the harmonic oscillator model. Therefore, the new C−D vibrations are located in the spectral range 2300−2000 cm^{-1}, a spectral region free of interference from other vibrational modes and easily observed spectroscopically via IRRAS.

IRRAS Spectra of an Ideal Mixture. The C−H and C−D stretching regions of the surface pressure-dependent IRRAS spectra of an ideally mixed 1:2 DPPC/DPPC-d_{62} monolayer are presented in Figure 1 parts A and B, respectively. Clearly evident in the spectra in Figure 1A are the CH$_2$ ν_a band (~2920 cm^{-1}), the CH$_2$ ν_s band (~2850 cm^{-1}), and the CH$_3$ ν_a (~2960 cm^{-1}). The CH$_3$ ν_s band (~2870 cm^{-1}) is overlapped by the CH$_2$ ν_s band. The CH$_2$ ν_a band is complicated by overlapping contributions of broad Fermi resonance bands.[42,43] Clearly evident in the spectra in Figure 1B are the CD$_2$ ν_a band (~2195 cm^{-1}), the CD$_2$ ν_s band (~2090 cm^{-1}), and the CD$_3$ ν_a (~2220 cm^{-1}). The CD$_3$ ν_s fundamental (~2070 cm^{-1}) is observed as a shoulder on the lower frequency side of the CD$_2$ ν_s band. The small band at ~2160 cm^{-1} is assigned to the Fermi resonance interaction between CD$_3$ ν_s and a deformation overtone.[44] Similar band assignments are made for C−H and C−D stretching regions of the IRRAS spectra for the 1:2 DLiPC/DPPC-d_{62} monolayer presented in Figure 2.

A large change in intensity is observed in both the C−H and the C−D stretching regions as the DPPC and the DPPC-d_{62} components of the monolayer pass through the (LE−LC) phase transition. Isotherms for DPPC and DPPC-d_{62} on pure water at room temperature have previously been presented.[45−47] A shift of the peak maxima to lower wavenumbers with a concurrent
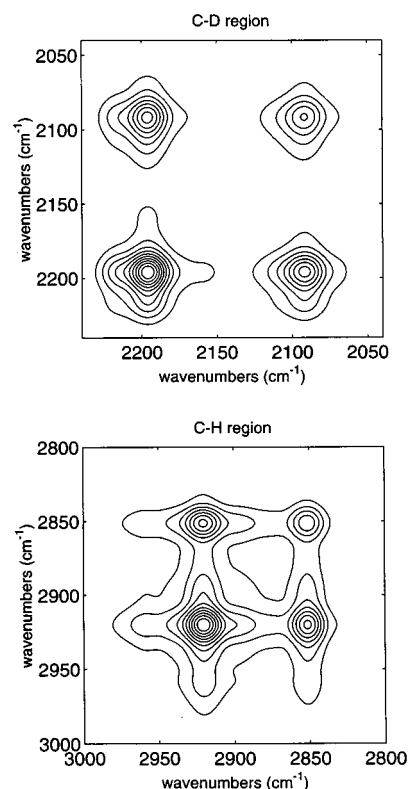

Figure 3. 2D IR synchronous correlation analysis plot for the ideal binary monolayer (1:2 DPPC/DPPC-d_{62}) spread at the air−water interface. The spectra were collected as a function of monolayer surface pressure and have been normalized for changes in surface density. (Top) The C−D stretching region representing the synchronous correlations from the DPPC-d_{62} component in the binary monolayer. (Bottom) The C−H stretching region representing the synchronous correlations from the DPPC component in the binary monolayer.

decrease in bandwidth is observed as the surface pressure increases. Specifically, the ν_a CH$_2$ band maximum shifts from 2925.5 to 2922.4 cm^{-1}, whereas the ν_s CH$_2$ band maximum shifts from 2856.2 to 2853.2 cm^{-1}. Likewise, the ν_a CD$_2$ band maximum shifts from 2198.3 to 2195.6 cm^{-1}, whereas the ν_s CD$_2$ band maximum shifts from 2098.9 to 2091.1 cm^{-1}.

IRRAS Spectra of a Nonideal Mixture. In the nonideal 1:2 DLiPC/DPPC-d_{62} mixture, the ν_a CH$_2$ band maximum that is due to the DLiPC acyl chains shifts only a small amount from 2920.4 to 2919.8 cm^{-1}, whereas the ν_s CH$_2$ band maximum similarly shifts only minimally from 2851.5 to 2851.4 cm^{-1}. On the other hand, the ν_a CD$_2$ band maximum that is due to the DPPC-d_{62} acyl chains shifts from 2198.3 to 2195.4 cm^{-1}, whereas the ν_s CD$_2$ band maximum shifts from 2098.1 to 2090.5 cm^{-1}. The position and the frequency shift of the CH$_2$ bands for DLiPC indicate a constant, highly ordered condensed phase component that changes little during the transition, whereas the position and the frequency shift of the CD$_2$ bands of DPPC-d_{62} indicate the ordering of an expanded phase component.

The shift of methylene stretching bands to lower wavenumbers has long been used to distinguish hydrocarbon order in a variety of alkane systems.[42] The magnitude of the wavenumber shifts for the CH$_2$ and CD$_2$ modes seen in Figures 1 and 2 are consistent with previously reported values for liquid expanded and liquid condensed phospholipid monolayer systems.[48,49]

2D IR Correlation Analysis. The standard synchronous 2D IR plots for the ideal and nonideal monolayer mixtures are presented in Figures 3 and 4, respectively. In both cases, only positive correlation intensities are observed in the 2D plots,
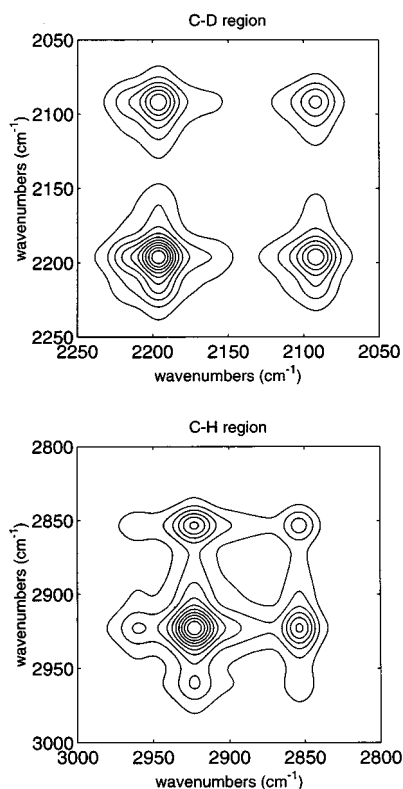
Figure 4. 2D IR synchronous correlation analysis plot for the nonideal binary monolayer (1:2 DLiPC/DPPC-d$_{62}$) spread at the air−water interface. The spectra were collected as a function of monolayer surface pressure and have been normalized for changes in surface density in the binary monolayer. (Top) The C−D stretching region representing the synchronous correlations from the DPPC-d$_{62}$ component. (Bottom) The C−H stretching region representing the synchronous correlations from the DLiPC in the binary monolayer.

indicating that all of the band intensities for the CH$_2$ and the CD$_2$ stretching regions are varying in the same direction. Large cross-peaks appear in a synchronous 2D IR correlation plot when two vibrational signals vary in a similar manner, or more specifically, with a large in-phase component.[1,2,4] In both Figures 3 and 4, the largest cross-peaks are observed for the bands at ∼2920 and 2850 cm^{-1}, thus indicating that the CH$_2$ ν_a and the CH$_2$ ν_s vary in a very similar manner, as expected. The auto-correlation intensities (i.e., the self-correlation intensities along the diagonal from the bottom left to the top right of the 2D plot) indicate the relative extent to which the various vibrational signals vary as the sample is perturbed.

The standard asynchronous 2D IR correlation analysis plots for the ideal and nonideal monolayer mixtures are presented in Figures 5 and 6, respectively. The asynchronous 2D plots have a much more complicated appearance than the synchronous 2D plots. This is because the cross correlation intensities are observed when two vibrational signals vary in a dissimilar or out-of-phase manner.[1,2,4] Because of this property, asynchronous 2D IR plots can provide enhanced resolution when compared to conventional IR spectra.

Prominent cross-peaks are observed in Figure 5 at approximately 2960, 2925, 2915, 2905, 2855, and 2850 cm^{-1} for the C−H region of the ideal monolayer mixture (Figure 5, bottom), whereas less prominent correlation features (humps) are observed at approximately 2890 and 2870 cm^{-1}. The cross-peaks at ∼2915 and 2925 cm^{-1} are assigned to two separable components of the CH$_2$ ν_a and are attributed to the coexisting ordered and disordered conformational states of the monolayer film, respectively. In an analogous manner, the cross-peaks at
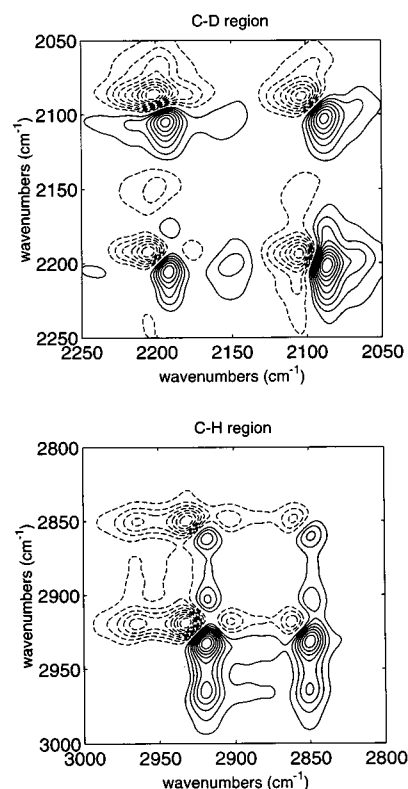

Figure 5. 2D IR asynchronous correlation analysis plot for the ideal binary monolayer (1:2 DPPC/DPPC-d$_{62}$) spread at the air−water interface. The spectra were collected as a function of monolayer surface pressure and have been normalized for changes in surface density. (Top) The C−D stretching region representing the asynchronous correlations from the DPPC-d$_{62}$ component. (Bottom) The C−H stretching region representing the asynchronous correlations from the DPPC component.

∼2850 and 2855 cm^{-1} are assigned to two separable components of the CH$_2$ ν_s and are attributed to the coexisting ordered and disordered conformational states of the film, respectively. We have previously considered the details of the appearance of these cross-peaks and how 2D IR can discern coexisting ordered and disordered conformational states in a monolayer film.[30,31] The 2D IR correlation plots presented here for the binary mixtures are analogous to those we have previously presented for single monolayer films. The other cross-peak assignments are presented in Table 1, and the basis for these assignments will be given in the next section ($\beta\nu$ Correlation Analysis).

In Figure 5 prominent cross-peaks are also observed at approximately 2205, 2195, 2175, 2150, 2105, 2095, and 2065 cm^{-1} for the C−D region, whereas less prominent correlation features (humps) are observed at approximately 2220 and 2070 cm^{-1} (Figure 5, top). Using the same reasoning as given above for the C−H region, the cross-peaks at ∼2195 and 2205 cm^{-1} are assigned to the ordered and disordered components of the CD$_2$ ν_a, respectively, whereas the cross-peaks at ∼2095 and 2105 cm^{-1} are assigned to the ordered and disordered components of the CD$_2$ ν_s, respectively. Inspection of Figure 5 shows that the CD$_2$ ν_a and ν_s cross-peaks in the C−D region show the same type of behavior as do the CH$_2$ ν_a and ν_s cross-peaks in the C−H region, further confirming the ideal mixing behavior of this binary system.

Assuming that the cross-peak at ∼2175 cm^{-1} is a deuterated analogue of ∼2905 cm^{-1}, the cross-peak at ∼2175 cm^{-1} may tentatively be assigned to a CH$_3$ Fermi resonance band or a CH$_3$ deformation overtone. The basis for this assignment is given in the next section. The cross-peak observed at ∼2155 cm^{-1} is
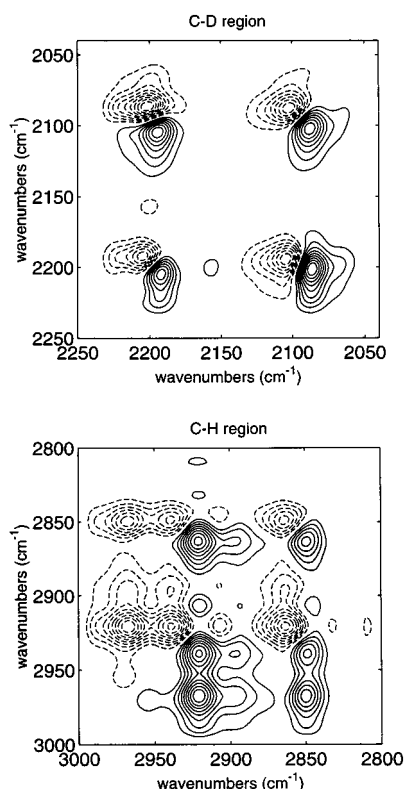
A Study of Binary Phospholipid Mixtures

J. Phys. Chem. A, Vol. 106, No. 14, 2002 **3425**

Figure 6. 2D IR asynchronous correlation analysis plot for the nonideal binary monolayer (1:2 DLiPC/DPPC-d_{62}) spread at the air–water interface. The spectra were collected as a function of monolayer surface pressure and have been normalized for changes in surface density. (Top) The C–D stretching region representing the asynchronous correlations from the DPPC-d_{62} component in the binary monolayer. (Bottom) The C–H stretching region representing the asynchronous correlations from the DLiPC component in the binary monolayer. Note: For comparison purposes, the absolute correlation intensities for the nonideal mixture (this figure) are approximately 10× lower than that of the ideal mixture shown in Figure 5.

TABLE 1: Band Assignments and Effective Phase Angle Values (b_e) for the Ideal and the Nonideal Mixtures

		β_e values	
$\sim\nu$ (cm^{-1})[a]	band[b]	ideal	Nonideal
2960 (m)	ν_a CH$_3$	227.2	34.7
2940 (w)	FR ν_s CH$_3$	225.0	52.7
2870 (m)	ν_s CH$_3$	224.2	50.5
2850 (s)	ν_s CH$_2$	221.1	179.0
2904 (w)	FR w CH$_3$ or 2δ **CH$_3$**	221.0	107.3
2890 (w)	FR w *NO* CH$_3$	219.5	164.3
2916 (s)	ν_a CH$_2$	218.6	160.1
2194 (s)	ν_a CD$_2$	218.7	195.2
2089 (s)	ν_s CD$_2$	217.0	192.0

[a] The symbols s, m, w, and v represent strong, medium, weak, and very, respectively. [b] The symbols ν an**d** d represent stretch and bend. FR represents Fermi resonance.

assigned to Fermi resonance interaction between CD$_3$ ν_s and a deformation overtone.[44] The correlation features observed at ∼2220 and 2070 cm^{-1} are assigned to CD$_3$ ν_a and ν_s fundamentals, respectively.

In Figure 6, prominent cross-peaks are observed at approximately 2960, 2940, 2920, 2905, 2890, 2870, and 2850 cm^{-1} for the C–H region for the nonideal monolayer mixture (Figure 6, bottom). The assignment of these cross-peaks to specific vibrational modes is presented in Table 1. The basis for these assignments is discussed in the next section. The cross-peak

assignments in the C–D region for the nonideal mixture are the same as the cross-peak assignments in the C–D region for the ideal mixture (Figure 6, top).

Interpretation of the 2D IR asynchronous correlation map for the nonideal binary mixture follows the same reasoning presented above for the ideal mixture. The cross-peaks observed in Figure 6 illustrate the coexisting nature of ordered and disordered components in each of the components in the monolayer film. Therefore, using the cross-peaks in the 2D IR asynchronous maps, we are able to identify the presence of crystalline solid and noncrystalline disordered regions in the monolayer. However, we are not able to reach any conclusions concerning the dynamics of how these structures change upon sample perturbation based solely on the standard 2D IR correlation plots. For such an analysis, we turn to $\beta\nu$ correlation analysis.

$\beta\nu$ Correlation Analysis. The basis of the $\beta\nu$ correlation analysis involves performing an asynchronous cross correlation between a dynamic spectral variation, $y(\nu,n)$, against a simple sinusoid mathematical function. The output correlation intensities of such an analysis are a function of the spectral frequency (ν) and the phase angle (β) of the sinusoidal function. The maximum positive correlation intensity will be observed at one point (ν,β) in the correlation plot for the range $360° \geq \beta \geq 0°$. This point is used to define a new parameter: the *effective phase angle* β_e of $y(\nu,n)$. The effective phase angle, β_e, is simply equal to $\beta + 90°$ at this point. In graphical terms, β_e is the point of maximum positive correlation intensity in the β vs ν plot. The β_e value quantitatively reveals the temporal relationships and the degree of coupling between the signal variations in a set of dynamic spectra. Some other desirable properties of $\beta\nu$ correlation analysis include the following: (1) $\beta\nu$ correlation plots are relatively easy to calculate in that they require no Fourier transformations; (2) the effective phase angle, β_e, is a direct result of the correlation analysis; therefore, no additional calculations are required; (3) in appropriate situations, β_e values from different experiments may be compared; and (4) noise is observed at a lower level in a $\beta\nu$ correlation plot than the standard 2D IR maps. A detailed description of $\beta\nu$ correlation analysis is presented elsewhere.[14]

The $\beta\nu$ correlation plots for the C–H and C–D stretching regions of the 1:2 DPPC/DPPC-d_{62} binary monolayer are shown in Figure 7. The β_e values and the band assignments for this ideally miscible monolayer obtained from Figure 7 are presented in Table 1. It is immediately apparent from Figure 7 that all of the methyl and the methylene components of the C–H stretching regions have similar β_e values, i.e., $\beta_e = \sim220°$ (Figure 7, bottom). Figure 7 also reveals that all of the methyl and the methylene components of the C–D stretching regions have β_e values of ∼220° (Figure 7, top). These results confirm the miscible, ideal nature of the DPPC/DPPC-d_{62} monolayer by suggesting that the acyl chains of both components react identically to surface pressure changes.

The $\beta\nu$ plots for the C–H and C–D stretching regions of the 1:2 DLiPC/DPPC-d_{62} binary monolayer are shown in Figure 8. The β_e values and the band assignments for this nonideal, immiscible monolayer are also presented in Table 1. In contrast to the $\beta\nu$ plots for the 1:2 DPPC/DPPC-d_{62} monolayer, the C–H and C–D stretching regions are quite different for the 1:2 DLiPC/DPPC-d_{62}monolayer. The C–D methyl and the C–D methylene stretching bands in the DPPC-d_{62} component have similar β_e values of ∼200° (Figure 8, top). In Figure 8 (top), a weak correlation peak (∼10% of the maximum correlation intensity) appears near 2100 cm^{-1} with a β_e value of ∼360°.
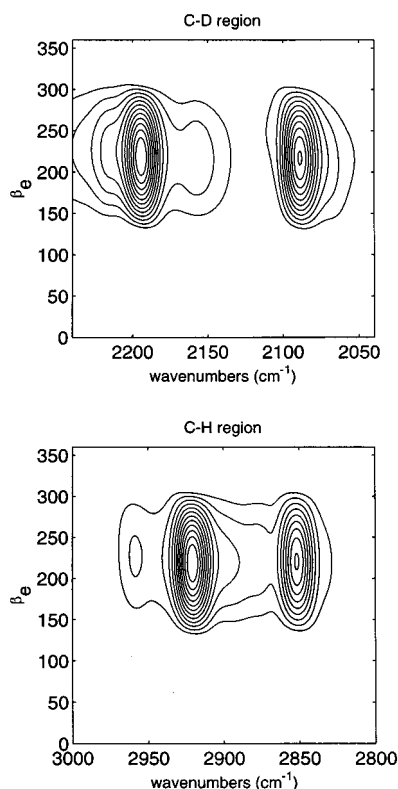
Figure 7. $\beta\nu$ correlation analysis plot for the ideal binary monolayer (1:2 DPPC/DPPC-d$_{62}$) spread at the air−water interface. The spectra were collected as a function of monolayer surface pressure and have been normalized for changes in surface density. (Top) The C−D stretching region representing the $\beta\nu$ correlations from the DPPC-d$_{62}$ component in the binary monolayer. (Bottom) The C−H stretching region representing the $\beta\nu$ correlations from the DPPC component in the binary monolayer.

The β_e value of this feature is nearly antiphase with the CD$_2$ ν_s band at ∼2090 cm^{-1} ($\beta_e \approx 195°$) and is therefore attributed to the disordered phase in the DPPC-d$_{62}$ component.[30,31] If enough contour levels are used, this feature also appears in the $\beta\nu$ plot for the C−D stretching region of the 1:2 DPPC/DPPC-d$_{62}$ ideally mixed monolayer (Figure 7, top).

In contrast with the C−D modes, however, the β_e values for the C−H methyl vibrations differ dramatically from the β_e values for the C−H methylene vibrations in the DLiPC component (Figure 8, bottom). Specifically, the β_e values of the methyl bands are ∼50°, whereas the β_e values of the methylene bands are ∼175° for DLiPC component. In a case where the methylene and the methyl bands are resolved, we would expect to see three methyl bands, i.e., the CH$_3$ ν_a fundamental at ∼2960 cm^{-1}, the CH$_3$ ν_s Fermi resonance band at ∼2940 cm^{-1}, and the CH$_3$ ν_s fundamental at ∼2870 cm^{-1}.[42,43] (The CH$_3$ band near ∼2940 cm^{-1} is due to the Fermi resonance interaction between the CH$_3$ ν_s fundamental and the overtone of a CH$_3$ deformation mode.) We would also expect to see at least three methylene bands, i.e., the CH$_2$ ν_a fundamental at ∼2920 cm^{-1}, the CH$_2$ ν_s Fermi resonance band at ∼2890 cm^{-1}, and the CH$_2$ ν_s fundamental at ∼2850 cm^{-1}.[42,43] (The CH$_2$ band near 2890 cm^{-1} is due to the Fermi resonance interaction between the CH$_2$ ν_s fundamental and the overtone of a CH$_2$ deformation mode.) Indeed, all six bands are present in the $\beta\nu$ plot for the DLiPC component (Figure 8, bottom). A weak band also appears to exist at ∼2904 cm^{-1}; this band has a β_e value (∼107.3°) which is smaller than the average β_e value (∼168°) for the three methylene bands listed above. This band is therefore
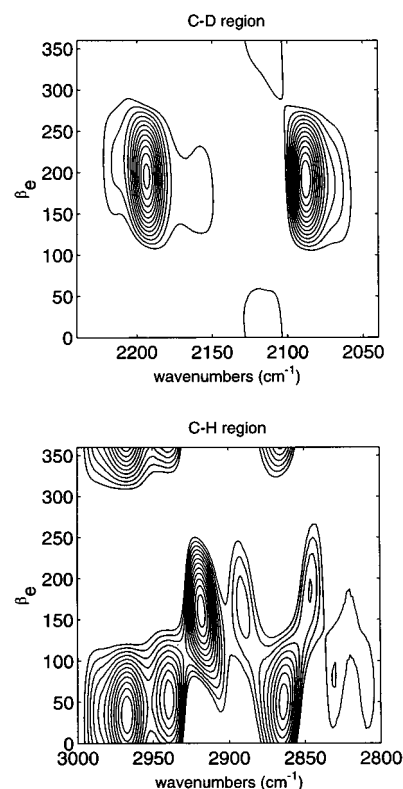

Figure 8. $\beta\nu$ plot for the nonideal binary monolayer (1:2 DLiPC/DPPC-d$_{62}$) spread at the air−water interface. The spectra were collected as a function of monolayer surface pressure and have been normalized for changes in surface density. (Top) The C−D stretching region representing the $\beta\nu$ correlations from the DPPC-d$_{62}$ component in the binary monolayer. (Bottom) The C−H stretching region representing the $\beta\nu$ correlations from the DLiPC component in the binary monolayer.

tentatively assigned to methyl Fermi resonance interactions or an overtone of a methyl deformation mode.

The differing β_e values for the methyl bands and the methylene bands in DLiPC can be explained by considering the location of gauche defects in the acyl chains of a condensed phase monolayer film. In a partial deuteration IRRAS study of condensed phase phospholipids and fatty acids at the A/W interface, Gericke, et al. showed that the gauche defects in the acyl chains are more concentrated in the half of the acyl chain containing the terminal methyl group than in the lower half of the chain adjacent to the interface.[49,50] Transmission IR studies of gel-phase phospholipid vesicles have shown that the gauche defects are also concentrated near the terminal methyl groups.[51,52] In the current study, both acyl chains of the DLiPC component of the mixed monolayer can be described as approximately all-trans with some gauche defects located near the terminal methyl groups. As the monolayer is compressed from 9.0 to 25.0 mN/m, a large amount of ordering takes place at the tail end of the acyl chain, which results in a large change in the orientation of the average methyl dipole-transition moment. Because the experiment is ∼75% s-polarized, these changes in orientation of the dipole-transition moment are detected as intensity variations in the methyl bands. In contrast, the intensity variation of the average methylene band is attributed to the slight change in tilt angle of the approximately all-trans acyl chains. The latter claim seems especially reasonable for a phospholipid like DLiPC, which contains a relatively large number of methylene groups. Both acyl chains in the DLiPC contain 22 methylene groups. Only a few of these 22 methylene groups are located in the gauche defect of an otherwise all-trans acyl chain;

A Study of Binary Phospholipid Mixtures

J. Phys. Chem. A, Vol. 106, No. 14, 2002 **3427**

TABLE 2: b_e Values for the Methylene Stretching Modes for Each Component of the Ideal and the Nonideal Mixtures

	b_e values			
band[a]	ideal	avg.	nonideal	avg.
ν_s CH$_2$	221.1	220	179.0	170
ν_a CH$_2$	218.6		160.1	
ν_a CD$_2$	218.7	218	195.2	194
ν_s CD$_2$	217.0		192.0	

therefore, the average methylene group exists in an approximately all-trans conformation. It then follows that the changes in IR intensity for the methylene stretching vibrations may simply be attributed to changes in tilt angle of the molecular axis as the monolayer is compressed. In summary, as the ideal and nonideal monolayer mixtures are compressed, conformational ordering takes place throughout the acyl chain of the DPPC and the DPPC-d$_{62}$ components, whereas ordering mostly takes place near the terminal methyl group of the acyl chain of the DLiPC component.

The β_e values can be used to determine the relative rates of IR intensity change as a compound undergoes a phase transition.[14] The β_e values for the CH$_2$ and CD$_2$ stretch bands of the ideal and nonideal monolayer mixtures are presented in Table 2. The mean β_e value for the symmetric and anti-symmetric CH$_2$ and CD$_2$ stretching vibrations is used to determine relative rates of intensity change for the average CH$_2$ or CD$_2$ band in each component. The β_e values from a duplicate experiment differed by only a few degrees.

The β_e data obtained from Table 2 can be used to make the following observations. First, the intensity changes for the CH$_2$ and CD$_2$ stretch bands of the DPPC and DPPC-d$_{62}$ components of the ideal mixture have approximately equal rates ($\beta_e = 220°$ for CH$_2$ and $\beta_e = 218°$ for CD$_2$). Second, the intensity changes for the CH$_2$ and CD$_2$ stretching vibrations of the ideal mixture ($\beta_e = 220°$) are different from the intensity changes of the CD$_2$ stretching vibrations of the nonideal mixture ($\beta_e = 194°$). Therefore, the rate of change is larger for the CH$_2$/CD$_2$ bands of the ideal mixture than for the CD$_2$ bands of the DPPC-d$_{62}$ component of the nonideal mixture. Finally, the intensity changes for the CH$_2$ bands for the DLiPC component ($\beta_e = 170°$) and the CD$_2$ bands for the DPPC-d$_{62}$ component ($\beta_e = 194°$) of the nonideal mixture are different; i.e. the rate of change is larger for the CD$_2$ bands of DPPC-d$_{62}$ than for the CH$_2$ bands of DLiPC. From the data in Table 2, the relative rates of IR intensity change for these two mixtures can be summarized as the following: CH$_2$ for ideal mixture ($\beta_e = 220°$) $\approx$ CD$_2$ for ideal mixture ($\beta_e = 218°$) > CD$_2$ for nonideal mixture ($\beta_e = 194°$) > CH$_2$ for nonideal mixture ($\beta_e = 170°$).

The relative rates of change in IR intensity for the methylene bands are interpreted as relative rates of conformational ordering (i.e., gauche $\rightarrow$ trans isomerization) in the acyl chains of the mixed monolayer films. This interpretation is consistent with the known interpretation of the frequency shifts of the CH$_2$ and CD$_2$ vibrational modes, as well as with the known surface chemistry for these binary monolayers. For example, the acyl chains for the DPPC:DPPC-d$_{62}$ system respond identically to surface pressure and become ordered at the same rate, as expected for a miscible, ideal mixture. In addition, the acyl chains of both components in the ideal mixture become ordered at a faster rate than the DPPC-d$_{62}$ component of the nonideal mixture. This is also consistent with the observation of a broadened phase transition in the pressure−area isotherm for the nonideal monolayer mixture as compared to the isotherm for the ideally mixed monolayer. Finally, in the nonideal mixture, the acyl chains of the DPPC-d$_{62}$ component become

ordered at a faster rate than the acyl chains of the DLiPC component. Again, this is consistent with the data from the IR spectra that show that the DLiPC component is relatively ordered at all surface pressures (9.0−25.0 mN/m). In the DLiPC/DPPC-d$_{62}$ mixture, it is mainly the DPPC-d$_{62}$ component that responds to surface pressure perturbation with frequency shift and band intensity changes, as illustrated in Figure 2.

Conclusions

Ideal and nonideal mixtures of phospholipids were studied as monomolecular films at the A/W interface using IRRAS and $\beta\nu$ correlation analysis. This study shows for the first time that the methyl stretching modes in IRRAS spectra can be used as in situ indicators of structural dynamics in the acyl chains of a Langmuir monolayer. Methyl (2940 cm^{-1}) and methylene ($\sim$2890 cm^{-1}) Fermi resonance bands are clearly resolved from the fundamental bands in the C−H stretching region of the $\beta\nu$ plot for the nonideal mixture. Similar β_e values are observed for the methyl and the methylene stretching bands in the DPPC component of the ideal mixture. The same situation is observed for the DPPC-d$_{62}$ component in the ideal mixture and the DPPC-d$_{62}$ component in the nonideal mixture. In contrast, dissimilar β_e values are observed for the methyl and the methylene stretching bands of the DLiPC component of the nonideal mixture. This observation can be explained by considering the location of gauche defects in the acyl chains of the individual components. As the ideal and nonideal monolayer mixtures are compressed, conformational ordering takes place throughout the acyl chains of the DPPC and the DPPC-d$_{62}$ components, whereas ordering mostly takes place near the terminal methyl groups of the acyl chain of the DLiPC component. The β_e values can therefore be used to determine the relative rates of conformational ordering in the individual components of the two monolayer systems.

References and Notes

(1) Noda, I. *Appl. Spectrosc.* **1990**, *44*, 550−554.

(2) Noda, I. *Appl. Spectrosc.* **1993**, *47*, 1329−1336.

(3) Harrington, P. D.; Urbas, A.; Tandler, P. J. *Chemom. Intell. Lab. Syst.* **2000**, *50*, 149−174.

(4) Noda, I.; Dowrey, A. E.; Marcott, C.; Story, G. M.; Ozaki, Y. *Appl. Spectrosc.* **2000**, *54*, 236A-248A.

(5) Nabet, A.; Pezolet, M. *Appl. Spectrosc.* **1997**, *51*, 466−469.

(6) Noda, I.; Story, G. M.; Marcott, C. *Vib. Spectrosc.* **1999**, *19*, 461−465.

(7) Magtoto, N. P.; Sefara, N. L.; Richardson, H. H. *Appl. Spectrosc.* **1999**, *53*, 178−183.

(8) Hinterstoisser, B.; Salmen, L. *Vib. Spectrosc.* **2000**, *22*, 111−118.

(9) Sonoyama, M.; Miyazawa, M.; Katagiri, G.; Ishida, H. *Appl. Spectrosc.* **1997**, *51*, 545−547.

(10) Ozaki, Y.; Liu, Y.; Noda, I. *Appl. Spectrosc.* **1997**, *51*, 526−535.

(11) Ren, Y. Z.; Shimoyama, M.; Ninomiya, T.; Matsukawa, K.; Inoue, H.; Noda, I.; Ozaki, Y. *Appl. Spectrosc.* **1999**, *53*, 919−926.

(12) Wu, P.; Siesler, H. W. *J. Mol. Struct.* **2000**, *521*, 37−47.

(13) Ekgasit, S.; Ishida, H. *Appl. Spectrosc.* **1995**, *49*, 1243−1253.

(14) Elmore, D. L.; Dluhy, R. A. *J. Phys. Chem. B* **2001**, *105*, 11377−11386.

(15) Dluhy, R. A.; Cornell, D. G. *J. Phys. Chem.* **1985**, *89*, 3195−3197.

(16) Dluhy, R. A. *J. Phys. Chem.* **1986**, *90*, 1373−1379.

(17) Dluhy, R. A. Infrared spectroscopy of biophysical monolayer films at interfaces. Theory and Applications. In *Physical Chemistry of Biological Interfaces*; Baszkin, A., Norde, W., Eds.; Marcel Deker: New York, 2000; pp 711−747.

(18) Mendelsohn, R.; Brauner, J. W.; Gericke, A. *Annu. Rev. Phys. Chem.* **1995**, *46*, 305−334.

(19) Gericke, A.; Michailov, A.; Hühnerfuss, H. *Vib. Spectrosc.* **1993**, *4*, 335−348.

(20) Blaudez, D.; Buffeteau, T.; Cornut, J. C.; Desbat, B.; Escafre, N.; Pezolet, M.; Turlet, J. M. *Appl. Spectrosc.* **1993**, *47*, 869−874.

(21) Blaudez, D.; Buffeteau, T.; Desbat, B.; Turlet, J. M. *Curr. Opin. Colloid Interface Sci.* **1999**, *4*, 265−272.

(22) Dicko, A.; Bourque, H.; Pezolet, M. *Chem. Phys. Lipids* **1998**, *96*, 125−139.

(23) Möhwald, H. *Annu. Rev. Phys. Chem.* **1990**, *41*, 441−476.

(24) Knobler, C. M. *Adv. Chem. Phys.* **1990**, *77*, 397−449.

(25) Gericke, A.; Flach, C. R.; Mendelsohn, R. *Biophys. J.* **1997**, *73*, 492−499.

(26) Bellet-Amalric, E.; Blaudez, D.; Desbat, B.; Graner, F.; Gauthier, F.; Renault, A. *Biochim. Biophys. Acta* **2000**, *1467*, 131−143.

(27) Grandbois, M.; Desbat, B.; Blaudez, D.; Salesse, C. *Langmuir* **1999**, *15*, 6594−6597.

(28) Dluhy, R. A.; Reilly, K. E.; Hunt, R. D.; Mitchell, M. L.; Mautone, A. J.; Mendelsohn, R. *Biophys. J.* **1989**, *56*, 1173−1181.

(29) Buffeteau, T.; Desbat, B.; Pezolet, M.; Turlet, J. M. *J. Chim. Phys. Phys.−Chim. Biol.* **1993**, *90*, 1467−1489.

(30) Elmore, D. L.; Dluhy, R. A. *Appl. Spectrosc.* **2000**, *54*, 956−962.

(31) Elmore, D. L.; Dluhy, R. A. *Colloids Surf., A* **2000**, *171*, 225−239.

(32) Sakai, H.; Umemura, J. *Langmuir* **1997**, *13*, 502−505.

(33) Cameron, D. G.; Kauppinen, J. K.; Moffatt, D. *Appl. Spectrosc.* **1982**, *36*, 245−250.

(34) Noda, I. *Appl. Spectrosc.* **2000**, *54*, 994−999.

(35) Hansen, W. N. *J. Opt. Soc. Am.* **1968**, *58*, 380−390.

(36) Gericke, A.; Hühnerfuss, H. *J. Phys. Chem.* **1993**, *97*, 12899−12908.

(37) Phillips, M. C.; Ladbrooke, B. D.; Chapman, D. *Biochim. Biophys. Acta* **1970**, *196*, 35−50.

(38) Mabrey, S.; Sturtevant, J. M. *Proc. Natl. Acad. Sci. U.S.A.* **1976**, *73*, 3862−3869.

(39) Lee, A. G. *Biochim. Biophys. Acta* **1977**, *472*, 285−344.

(40) Dluhy, R. A.; Moffatt, D.; Cameron, D. G.; Mendelsohn, R.; Mantsch, H. H. *Can. J. Chem.* **1985**, *63*, 1925−1932.

(41) Rana, F. R.; Mautone, A. J.; Dluhy, R. A. *Appl. Spectrosc.* **1993**, *47*, 1015−1023.

(42) Snyder, R. G.; Hsu, S. L.; Krimm, S. *Spectrochim. Acta* **1978**, *34A*, 395−406.

(43) Snyder, R. G.; Strauss, H. L.; Elliger, C. A. *J. Phys. Chem.* **1982**, *86*, 5145−5150.

(44) Dluhy, R. A.; Mendelsohn, R.; Casal, H. A.; Mantsch, H. H. *Biochemistry* **1983**, *22*, 1170−1177.

(45) Hunt, R. D.; Mitchell, M. L.; Dluhy, R. A. *J. Mol. Struct.* **1989**, *214*, 93−109.

(46) Albrecht, O.; Gruler, H.; Sackmann, E. *J. Phys. (Paris)* **1978**, *39*, 301−313.

(47) Chung, J. B.; Hannemann, R. E.; Franses, E. I. *Langmuir* **1990**, *6*, 1647−1655.

(48) Dluhy, R. A.; Wright, N. A.; Griffiths, P. R. *Appl. Spectrosc.* **1988**, *42*, 138−142.

(49) Gericke, A.; Moore, D. J.; Erukulla, R. K.; Bittman, R.; Mendelsohn, R. *J. Mol. Struct.* **1996**, *379*, 227−239.

(50) Gericke, A.; Mendelsohn, R. *Langmuir* **1996**, *12*, 758−762.

(51) Mendelsohn, R.; Davies, M.; Brauner, J. W.; Schuster, H. F.; Dluhy, R. A. *Biochemistry* **1989**, *28*, 8934−8939.

(52) Casal, H. L.; McElhaney, R. N. *Biochemistry* **1990**, *29*, 5423−5427.